EFFECTS FROM MEASURED GROUND MOTIONS AT THE SSC

King-Yuen Ng
Fermi National Accelerator Laboratory Batavia, IL 60510, U.S.A.*
Jack M. Peterson
SSC Laboratory, Dallas, TX 75237, U.S.A.*

The separation of the two beams in the SSC caused by ground motion produced by railroad and highway traffic crossing over the ring and by nearby quarry blasts were estimated from measured amplitude spectra using a complete optical model of the accelerator lattice but a simplified model of the ground structure. The beam separation expected from the largest ground motion recorded from train crossings is only a few percent of the rms beam width at the beam-crossing points. However, beam separation caused by quarry blasts are larger and can momentarily produce significant loss in luminosity.

I. INTRODUCTION

Movement of the quadrupole magnets in the Superconducting Super Collider (SSC) affects the closed orbits of the two proton beams differently and so can cause the two beams to separate from each other at the crossing points in the interaction regions.[1] Recently, geophone measurements were made of the ground motion by K. Hennon and D. Hennon of the Earth Technology Corporation[2] at the planned SSC site, at 5 points where railroads and/or highways cross over the projected ring tunnel (Fig. 1). Several sets of data were taken near the surface and at the projected tunnel depth ranging from 20 to 75 m, most of which is in the Austin chalk. The impact of these data on beam separation is discussed below, and the details are given in Ref. 3.

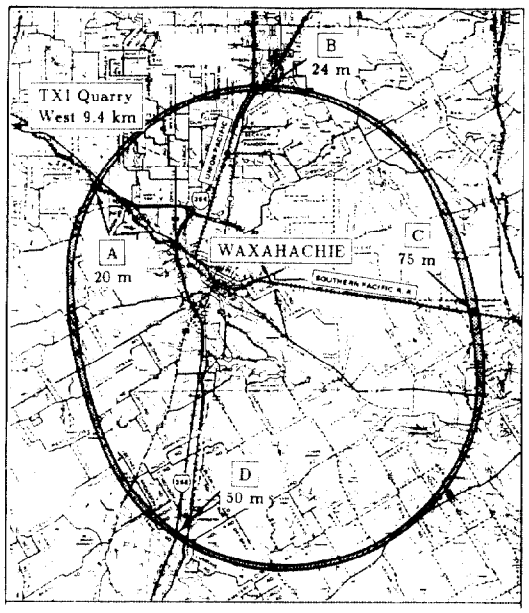

Fig. 1. Ground-motion measurements were made near the surface, near the top of the Austin chalk layer, and at the anticipated tunnel depth (indicated at each measuring site).

II. EXPERIMENTAL RESULTS

1. Largest recorded signals

A four-second interval of the largest recorded signal at tunnel depth due a train passing at Site A is shown in Fig. 2a. The corresponding displacement spectrum obtained by fast Fourier transform and application of the measured frequency response of the geophone used plus time integration to convert velocity to displacement is shown in Fig. 2b. Train spectra in other sets of measurement were similar. The largest recorded ground motion caused by highway traffic at tunnel depth was at least an order of magnitude smaller. A similar sample of the largest recorded signal produced through 4243 pounds of explosive at a quarry 9.4 km northwest of Site A is shown in Fig. 3a and the corresponding amplitude spectrum in Fig. 3b.

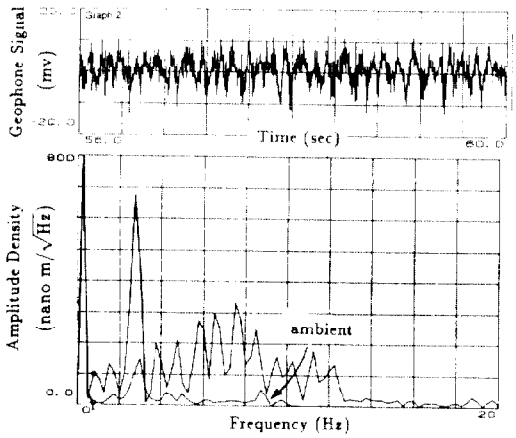

Fig. 2. (a) Largest of 17 train signals from geophone at tunnel depth (20 m) due to a train crossing overhead at Site A in the northwest arc. (b) Vibration amplitude spectrum obtained by a fast Fourier transform.

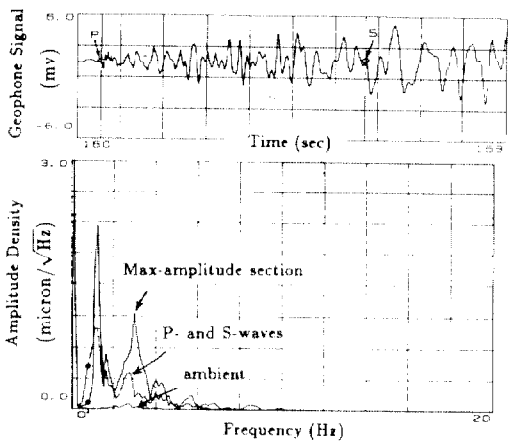

Fig. 3 (a) Geophone signal due to a quarry blast 9.4 km northwest recorded at tunnel depth at Site A. The maximum-amplitude section arrived at 173 s. (b) The amplitude spectrum obtained by a fast Fourier transform.

2. Properties of propagating medium

From the measured down-hole velocities of the compressional and shear waves, plus the measured material densities, the elastic constants, Poisson ratio, and velocity of dominant Rayleigh surface waves in the Austin chalk were inferred (Table I).

3. Attenuation

The attenuation of ground wave at frequency f due to absorption was assumed to follow the form e^{-fR/L_c}, where R is the horizontal distance from the source and L_c is the characteristic attenuation length.

*Operated by the Universities Research Association, Inc., under contracts with the U.S. Department of Energy.

	Velocities (km/s)			Poisson	Moduli ($\times 10^5$ psi)	
	longitud.	transv.	Rayleigh	ratio	Young's	shear
surface	1.1-1.5	.63-.89	.58-.81	0.17-0.38	3.1-5.7	1.2-2.5
tunnel	1.7-2.7	1.0-1.6	.90-1.5	0.25-0.35	7.9-19.0	3.2-7.8
blast	3.3	1.4	1.3	0.39	16.7	6.0

Table 1: Results from down-hole and quarry blast velocity measurements in the Austin stratum (density 2.16 gm/cm^3).

Three determinations of L_c were made: (1) From the train distance at which the geophone signal became apparent relative to the ambient noise, L_c ranging from 0.7 to 2.5 km/Hz were obtained, with best data favoring 1.0 km/Hz. (2) From the two bore holes at Site B, one directly below the train crossing and the other some 200 m away, $L_c \approx 5$ km/Hz was obtained. (3) From measurement of the relative amplitudes of ground waves from a quarry blast at two well-separated sites (one pair were Sites A and B, 9.4 and 19.5 km from the quarry, the other pair were Sites A and C, 9.4 and 33.4 km away), $L_c \approx 10$ km/Hz was determined.

The shorter attenuation lengths obtained from the train data is interpreted as due partly to the greater absorption in the relatively soft alluvial deposits in which the railroad tracks are imbedded and partly to the reflections of the ground waves at the alluvial/Austin-chalk interface. Differing effective thickness of the alluvial deposits could account for the different attenuation lengths derived from the first two methods.

III. SIMULATION

1. The model

The closed-effects due to the motion of each quadrupole in the complete SSC lattice (September 1987 version) were computed. The SSC site, however, was modeled simply as a uniform, homogeneous, semi-infinite block of Austin chalk.[1] The source of ground waves for the blast was a single point source vibrating on the surface of the quarry site. The train model consisted of 48 such vibrating points with random phases over a length of 960 m along the railroad that crosses over the northwest section of the ring where the tunnel depth is only 20 m. At each frequency of interest, the amplitudes of the ground waves were computed at a measuring site as well as at all quadrupole positions. Elastic constants of 2.6×10^6 psi in compression and 8.7×10^5 psi in shear, a Poisson ratio of 0.25, and a specific gravity of 2.0 for the Austin chalk give compressional, shear, and Rayleigh wave velocities of 3.0, 1.73, and 1.59 km/s, respectively. Although the model is much too simple, it was normalized to the amplitudes and frequency spectra measured by the Hennons[2] at the proper tunnel depths. We feel that the calculations of the resultant beam separations should be of the correct order of magnitude.

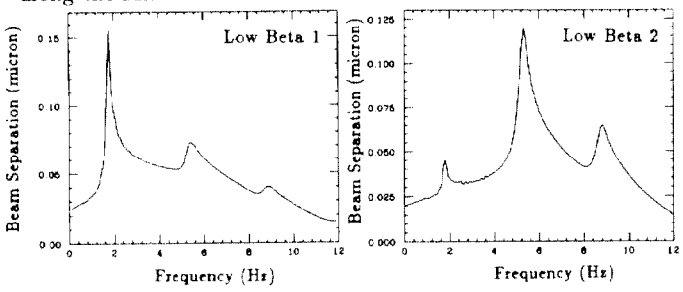

Fig. 4. Beam-separation spectra at the two low-beta crossings versus frequency of train vibrations for a characteristic attenuation length of 10 km.

2. Simulation results due to train crossing

The beam separations at the crossing points produced by train-induced ground vibrations vary considerably with the wavelength of the vibration, the position of the railroad crossing relative to the FODO lattice, and the attenuation encountered by the waves.

Figure 4 shows the calculated beam separation at the two low-beta crossings for a characteristic attenuation length of 10 km/Hz. The force function used to simulate crudely the train effects was flat from 0 to 5 Hz and then dropped with a Gaussian exponential with an rms width of 4 Hz. The beam separation at the two low-beta ($\beta^* = 0.5$ m) crossings show quite clearly the interference maxima that can occur when the ground wavelength is equal to the betatron wavelength and when it is equal to 1/3 and 1/5 of the betatron wavelength (1.8, 5.4, and 8.8 Hz, respectively). The separation spectra for the two crossings differ both in magnitude and in shape, partly due to the betatron phase difference between them, which is an odd multiple of 90°, and partly to the variation with frequency of the phase difference between each crossing and the effective center of the closed-orbit disturbance.

Figure 5 shows the variation of the beam-separation spectrum at one low-beta crossing with the value of the characteristic attenuation length. As the ground becomes more absorptive, fewer quadrupoles are effective in producing the total closed orbit, so that interference effects become much less pronounced.

Figure 6 shows the variation of the beam separation at the two low-beta crossings with position of the overhead railroad crossing along the 90° FODO lattice for the case of a 1 km/Hz attenuation length and at vibration frequencies of 2 Hz and 8 Hz. We note that the curves for the two crossings are identical except for relative shift of 90° and that they repeat at 180° intervals along the arc since only the absolute values of the separations are calculated. We have noted that the separation maxima occur in some cases when the train crossing is directly above a focussing quad (in the upper ring), and in other cases when it is above a defocussing quad, and in some cases when it is in between.

This displacement spectrum in Fig. 2b was simply integrated

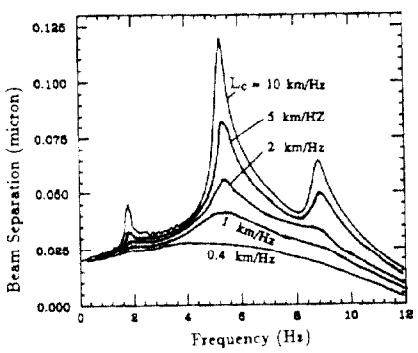

Fig. 5. The variation of the beam-separation spectrum due to a train crossing with different characteristic attenuation lengths.

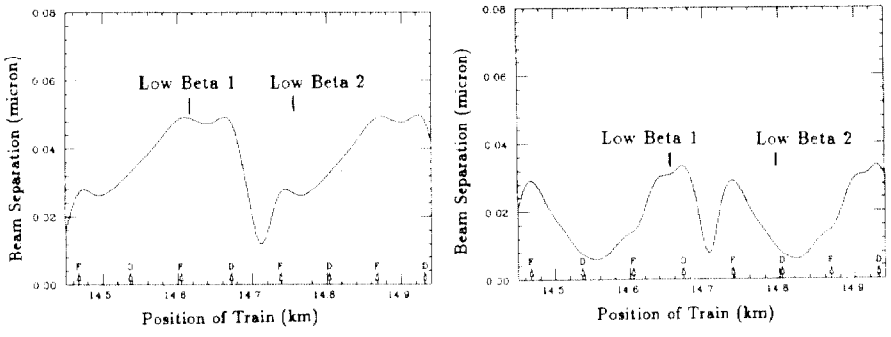

Fig. 6. The variation of the beam separation at the two low-beta crossings at a vibration frequency of (a) 2 Hz and (b) 8 Hz versus position of the overhead railroad crossing along the arc, with a characteristic attenuation length of 1 km/Hz.

to produced an approximate vertical ground motion amplitude of 0.55 micron in the 3-Hz component and a 0.58 micron amplitude at about 7 Hz. The phase information required for a Fourier reconstruction of the original time-dependent ground-motion wave form was not avaliable. We assumed that the "3-Hz" amplitude was at the betatron wavelength (1.8 Hz in the 1987 lattice) and that the broad "7-Hz" maximum was half at the $\lambda_\beta/3$ (5.4 Hz) and half at the $\lambda_\beta/5$ (8.8 Hz) resonances. We assumed also at each frequency and attenuation factor that the position of the train crossing was such as to maximize the separation at one the the beam crossings. The maximum separation expected at one of the low-beta crossings is obtained then by multiplying the vertical displacement at the measuring Site A by the maximum calculated beam separation per unit displacement at the same Site A each frequency component and attenuation constant of interest. The results are listed in Table II. The nominal rms beam width at $\beta^* = 0.5$ m is $\sigma = 4.8$ microns.

The luminosity at beam separation D is[4] $\mathcal{L} = \mathcal{L}_0 e^{-(D/2\sigma)^2}$, where $\mathcal{L}_0$ is the luminosity when the beams are well centered. If we assume that the separations given in Table II are increased by a factor of 5 due to magnet-support amplification (2-4 in HERA[5]), then the drop in luminosity in the worst case is only about 0.8%.

Measured δz_1		Calc. sep. δz_1			Separation at low-beta			
$f_1 = 3$ Hz	$f_2 = 7$ Hz	L_ϵ	at f_1	at f_2	at f_1	at f_2	total	
μ	μ	km/Hz	μ/μ	μ/μ	μ	μ	μ	σ
0.55	0.58	1	.091	.072	.050	.042	.092	.019
0.55	0.58	2	.123	.081	.068	.047	.115	.024
0.55	0.58	5	.188	.115	.103	.066	.169	.035

Table II: Maximum beam separation at a low-beta crossing due to a train-worst case.

3. Simulation results due to quarry blasts

The computed beam-separation spectra at the two low-beta crossings for a characteristic attenuation length of 10 km/Hz are shown in Fig. 7. The response of the system at low frequencies is relatively small until the ground wavelength approaches the average betatron wavelength of 1.8 Hz. These spectra were found not to change significantly when the quarry site was moved by 200 m in any direction.

The integrated displacement of the largest recorded blast at Site A (Fig. 3) was 1.4 micron near 1 Hz and 1.1 micron near 3 Hz. Since the "1-Hz" peak in the measured displacement spectrum extends well into the sharp rise of the computed beam-separation spectrum and because also of the many uncertainties in the effective properties of the Austin chalk, we evaluated the beam separation due to this peak as if it were half at 1 Hz and half at 2 Hz. The results are listed in Table III.

Thus, assuming an amplification factor of 5 due to quadrupole support, the maximum beam separation becomes 2.1 times the rms beam width, in which case the luminosity drops by 67%. Fortunately, quarry blasts took place only about 2 or 3 per week.

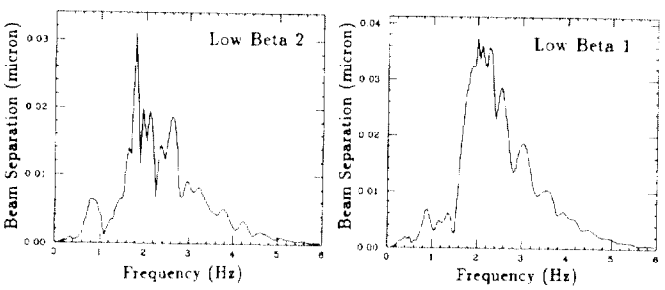

Fig. 7. Computed beam-separation spectra at the two low-beta crossings due to a point source at the quarry location, with a characteristic attenuation length of 10 km.

Measured δz_1		Calc. sep. δz_1			Separation at low-beta			
$f_1 = 1$ Hz	$f_2 = 3$ Hz	L_ϵ	at f_1	at f_2	at f_1	at f_2	total	
μ	μ	km/Hz	μ/μ	μ/μ	μ	μ	μ	σ
1.43	1.08	10	0.44	0.83	0.63	0.90	1.53	0.32
1.43	1.08	20	0.65	1.04	0.93	1.12	2.05	0.42

Table III: Maximum beam separation at a low-beta crossing due to a quarry-worst case.

IV. COMPENSATION OF BEAM SEPARATION

For compensating the transient beam separations at the interaction points, the automatic beam centering scheme outlined by Jostlein[4] should be workable. In this scheme, as indicated in Fig. 8, one beam is rotated at the crossing point with an amplitude b at a frequency $\omega/2\pi$ much higher than the characteristic frequencies of the error separation D that one wishes to correct. For b and D much smaller than the rms beam width σ, the luminosity varies as $\mathcal{L} = \mathcal{L}_0[1 - (b^2 + D^2)/4\sigma^2 - A\cos(\theta + \omega t)]$. A measurement of the modulating amplitude $A = 2bD/(4\sigma^2 - b^2 - D^2)$ gives the magnitude of the slowly varying separation D, and a Fourier analysis yields its direction θ.

We estimate the time to measure the two Fourier coefficients with a statistical accuracy of 10%. Assuming $b = 0.2\sigma$ (which produces only a 1% drop in average luminosity) and a luminosity counter that detects one-half of the events corresponding to a proton-proton cross section of 130 mb, the time to measure a beam separation D at the level where it produces a 1% drop in luminosity is only about 8 ms. A luminosity $\mathcal{L}_0 = 10^{37}$ m^{-2}sec^{-1} when the beams are well-centered is assumed. This speed of analysis of the beam separation is more than adequate, since significant ground motion was observed at highest frequencies around 10 Hz only.

To correct the measured beam separations, a local beam bump in each interaction region can be activated. The half-wave beam bumps can be produced by paris of small dipole corrector magnets located near the triplet quadrupole magnets. Since the betatron phase difference between the two triplet array is 180°, these locations are ideal for adjusting the beam position without affecting it anywhere else. To correct a beam separation equal to 1 rms beam width at the interaction points, the strengths of dipole correctors placed near the maximum-beta positions in the triplets need be only about 5.6×10^{-3} T-m in the low-beta interaction regions and 9.4×10^{-3} T-m in the medium-beta regions. The beta values at the correctors were assumed to be 7000 and 2400 m, respectively).

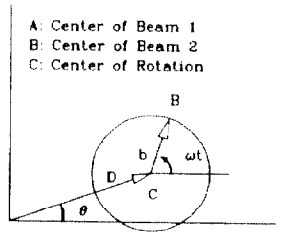

Fig. 8. Geometry of the beam-centering scheme with beam 1 centered at A. Beam 2 centered at B has a misalignment D at angle θ and rotates about C with a radius b and frequency $\omega/2\pi$.

REFERENCES

1. K. Ng and J. Peterson, SSC-212 Rev (FN-511), 1989.
2. K. & D. Hennon, Earth Technology Corporation, SSC-Sr-1043, Dec. 1989.
3. K. Ng and J. Peterson, SSC-277 (FN-543), 1990.
4. H. Jostlein, Fermilab Report TM-1253, 1984.
5. J. Rossbach, DESY Report, 1989.